Chemical Shrinkage Characterization during Curing through Three-Dimensional Digital Image Correlation

Kalima Bukenya, Sagar P. Shah, Alessandro Sabato, Marianna Maiarù*

University of Massachusetts Lowell, Lowell, MA 01854, USA

*Corresponding Author: marianna_maiaru@uml.edu

Abstract

Chemical shrinkage in thermosetting polymers drives residual stress development and induces residual deformation in composite materials. Accurate characterization of chemical shrinkage during curing is therefore vital to minimize residual stresses through process modeling and optimize composite performance. This work introduces a novel methodology to measure pre- and post-gelation chemical shrinkage of an epoxy resin using three-dimensional digital image correlation (3D-DIC). Differential scanning calorimetry (DSC) is employed to calculate reaction kinetics and correlate chemical shrinkage with degree of cure. Rheology experiments are conducted to quantify gelation and validate post-gelation. 3D-DIC post-gelation results show excellent agreement with rheology. Pre-gelation results show the effect of the in-situ curing in the proximity of constraints on the global strain behavior. This work introduced an innovative approach to characterize chemical shrinkage of thermosets during curing which will enable accurate residual stress prediction for enhancing thermoset composite performance and provided insight on the in-situ polymer behavior during processing.

1. Introduction

Thermosets composites are lightweight materials that enable energy efficient transportation and green energy production [1-3] and provide efficient solutions for high-strength and high-stiffness applications in engineering fields, including biomedical [4-8], civil infrastructure [9], automotive [10-12] and aerospace [13, 14]. Thermosetting polymer matrix composites (PMCs) undergo chemical shrinkage during the manufacturing (curing) process. Cure-induced chemical shrinkage is a driving factor of residual stress evolution in composite materials [15, 16]. Residual stress development leads to a decrease in composite performance [17-19]. Multiscale process modeling informed by accurate neat resin properties evolutions as a function of temperature and degree of cure enables accurate prediction of curing-induced residual stress and strength [3, 19]. Thus, accurate measurement of chemical shrinkage plays a key role in residual stress mitigation and performance optimization [3, 20-23]. Curing-induced shrinkage can result in residual shape distortion in 3D printed polymers [24, 25]. Thiol-ene photopolymerization is a widely applied method in the fabrication of optical devices with 3D printing [26]. In-space processing may reduce some cure-induced design problems [27]. However, nonuniform heating in space due to thermal radiation and solar irradiance presents a potential likelihood for shrinkage-induced distortion in polymers [28]. Graphene aerogels fabricated via hygrothermal reactions also encounter frequent large volume shrinkage [29].

Several experimental procedures have been developed over the years to characterize chemical shrinkage. Volume dilatometric methods derive chemical shrinkage from volume variation measured directly during testing [30-32]. Non-volume dilatometric techniques use contacting or non-contacting transducers to measure shrinkage [3, 33-35]. Nawab et al. provides a detailed evaluation of these different shrinkage characterization techniques and their effects [36]. Digital image correlation (DIC) is used in a wide range

of applications and shows promise as a contactless method for shrinkage measurement. Kravchenko et al. employed 2D-DIC to characterize post-gelation shrinkage [37]. This method was extended to 3D-DIC by Motagi et al. for shrinkage measurements in an autoclave environment [38]. Both methods adhered a printed speckle pattern to the resin for DIC image capture. Singer et al. applied a fine SiC powder directly to the liquid surface of two polymer-based adhesive anchor systems to capture the full cure shrinkage with 3D-DIC [39]. However, component strain information was not provided to ascertain the accuracy of out-of-plane measurements and shrinkage evolution with respect to degree of cure was not determined with this method.

In this study, 3D-DIC is employed with stereovision cameras to investigate the pre- and post-gelation shrinkage strains with respect to the degree of cure for thermosetting resin EPON 862 and curing agent TETA. Materials and experimental methods are discussed in Section 2. Results from 3D-DIC experiments are compared with rheology and discussed in Section 3. Major conclusions are drawn in Section 4.

2. Materials and Experimental Methods

This work focuses on EPON 862, a low-viscosity thermosetting resin produced by Westlake. Triethylenetetramine (TETA) was chosen as the curing agent to allow the resin to cure at room temperature for 3D-DIC observations. This material system (hereafter referred to as EPON 862/TETA) is mixed to a 100:14 stoichiometric ratio for all characterizations, as specified by the manufacturer data sheet.

2.1 Cure Kinetics

During curing, the resin, which is initially liquid, gradually solidifies while shrinking. The amount of solid phase as the reaction proceeds is quantified by the degree of cure, ϕ, that is defined as

$$\phi = \frac{H(t)}{H_T} \tag{1}$$

where $H(t)$ is the partial heat generated at time t, and H_T is the total heat of reaction at the end of the cure cycle. The rate of cure, $\frac{\mathrm{d}\phi}{\mathrm{d}t}$, can be defined mathematically as a function of temperature T and degree of cure:

$$\frac{\mathrm{d}\phi}{\mathrm{d}t} = f(T, \phi) \tag{2}$$

This function was expressed with a semi-empirical phenomenological kinetic model developed by Kamal et al. [40]:

$$f(T, \phi) = (K_1 + K_2\phi^m)(1 - \phi)^n \tag{3}$$

$$K_i = A_i \exp\left(-\frac{\Delta E_i}{RT}\right) \qquad i = 1,2 \tag{4}$$

where K_1 and K_2 are Arrhenius rate functions, m and n are dimensionless curve-fitting parameters, A_1 and A_2 are frequency-like constants, ΔE_1 and ΔE_2 are the activation energies, R is the universal gas constant, and T is the absolute temperature. Resin cure kinetics were measured using Differential Scanning Calorimetry (DSC) using procedures outlined in Shah et al. [3] and are found below in Table 1. DSC measurements enabled the correlation between the shrinkage evolution as a function of time and the evolution of solid phase during the reaction.

Table 1. Cure kinetic constants determined from isothermal DSC scans of EPON 862/TETA resin system.

Frequency-Like Constants [sec^{-1}]		Activation Energies [kJ/mol]		Curve-Fitting Exponents [-]	
A_1	A_2	ΔE_1	ΔE_2	m	n
242E+06	9.04E-02	72.5	11.5	0.92	1.75

2.2 Specimen Preparation

A schematic of the specimen preparation is found in Figure 1. The EPON 862 resin was degassed in a vacuum chamber for 15 minutes prior to introducing the TETA curing agent. The mixed EPON 862/TETA system was then degassed for an additional 15 minutes to remove any air bubbles induced by the mixing. The specimen container was then prepped while the resin mixture degassed. A Teflon sheet was fitted into a petri dish container to allow the resin to shrink freely. The newly degassed mixture was then poured into the prepped specimen container. A black spray-paint speckle pattern was applied to the mixture. Two sets of experiments were conducted that enabled the measurement of (1) the strain throughout the whole reaction and (2) only the resin shrinkage after gelation. The first experiment was performed by applying the speckle pattern immediately after pouring the resin while the polymer is still in viscous liquid form. This experiment set up requires in-depth understanding of the reaction kinetics, fast and careful application of the speckled pattern. The high exothermic reaction can induce the paint to melt or crack as the reaction proceeds. In the second case, a white coating layer was applied to the surface of the specimen upon gelation, approximately 40 minutes after the beginning of the mixing process, and subsequently, the black speckle pattern was applied.

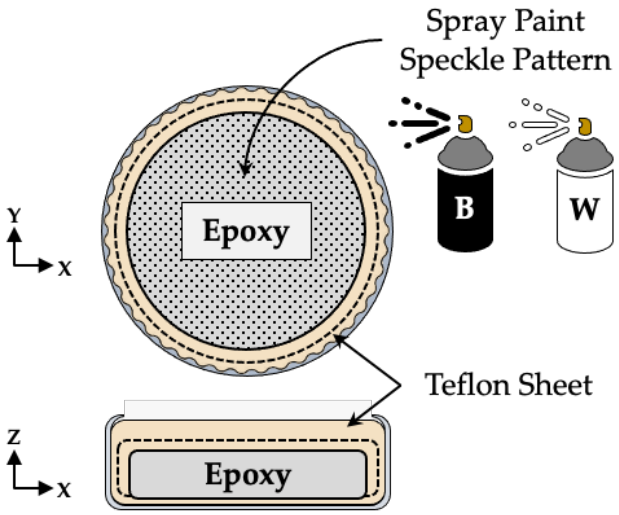

Figure 1. Schematic illustration of specimen preparation procedure.

2.3 3D-DIC Setup and Experiment

Three-dimensional Digital Image Correlation (3D-DIC) is a non-contact, full-field, photogrammetric measuring technique capable of extracting surface strain, displacement, and geometry profiles from images acquired through a synchronized stereo camera pair system [41]. 3D-DIC relies on tracking the displacement of a physical point P (with coordinates X_P, Y_P, Z_P in the global coordinate system X-Y-Z) on the surface of a targeted object between a reference state and altered configurations as it is represented in the camera coordinate system (i.e., the retinal plane x_i', y_i', 0 in pixel units) [42]. By combining the coordinates of the point P in the two cameras' retinal planes with the intrinsic and extrinsic parameters, the

physical position of point P in the 3D space can be obtained using triangulation [43]. A schematic of 3D-DIC is shown in Figure 2(a), while Figure 2(b) shows the 3D-DIC setup used in this study .

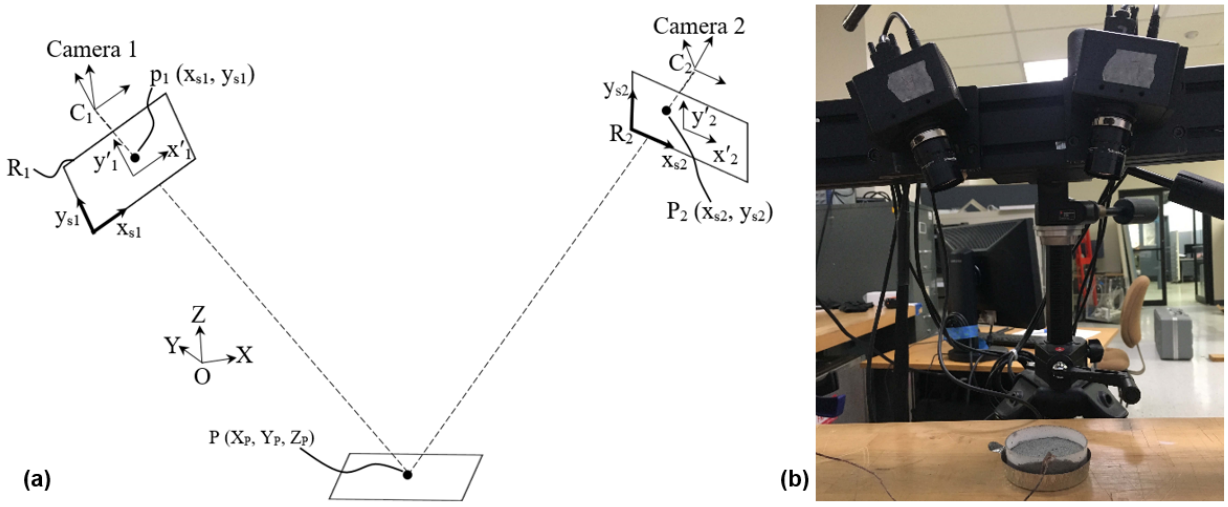

Figure 2. Pinhole camera model transformations of a schematic stereo cameras imaging setup for 3D-DIC (a) and experimental setup with trial run (b)

A stochastic pattern (e.g., black dots on a white background or vice versa) and/or optical targets need to be applied on the surface of interest, and the relative position of each target is tracked as the surface deforms over time. As an example, each image can be considered as a matrix of natural integers where white pixels have a grayscale level equal to 0 and black pixels with grayscale level 100 [44]. Because a single value in a pattern is not necessarily unique, a square neighborhood of pixels (i.e., facets or subsets) are used. Each facet is a set of distinctive correlation areas defined across the measuring region. Facets are usually 15-50-pixel square; thus, it includes several dots of the pattern. The center of each facet is a measurement point that can be thought of as an extensometer. The position of these facets is tracked through each of the successively acquired images, and the 3D coordinates of the entire area of interest are calculated. For all surface elements, the deformation gradient tensor **F** was introduced to map the undeformed line elements $d\mathbf{X}$ into the deformed line elements $d\mathbf{x}$:

$$d\mathbf{x} = \mathbf{F} \cdot d\mathbf{X} \tag{6}$$

The deformation gradient was then decomposed into two tensors such that:

$$\mathbf{F} = \mathbf{R} \cdot \mathbf{U} \tag{7}$$

where **R** is the rotation matrix and **U** is the right stretch tensor. Strain values were then recorded directly from the stretch tenor with the identity **I**:

$$\boldsymbol{\varepsilon} = \mathbf{U} - \mathbf{I} \tag{8}$$

The DIC system selected for performing this study consists of a pair of 2 Megapixel FWX201 series digital cameras manufactured by Baumer GmBH employing a 1/1.8” interline progressive charge coupled device (CCD) monochrome image sensors with a resolution of 1626 x 1236 pixels and a pixel size of 4.4 x 4.4 10-6 m [45]. The cameras were fitted with 12 mm focal length lenses manufactured by Schneider Optics, Inc. The 3D DIC system was positioned to have a working distance of ~32.0x10-2 m, a base distance of 12x10-2 m, and a separation angle of ~27°.

Figure 2(b) shows the test setup with the two cameras and a detail of the speckled epoxy specimen in a cup being tested. Due to the timing requested for performing the image acquisition, two different speckling procedures were employed during the tests. For the pre-gelation case, image acquisition started nearly ~15 minutes after the mixing process took place. For the post-gelation case, image acquisition started approximately 35 to 50 minutes depending on ambient temperature conditions.

For all tests performed, images were acquired every 30 seconds for the first hour of measurement and every 60 seconds for the following two hours. In this way, more information about the initial time of the curing process (i.e., when the reaction is faster) can be collected. It should be noticed that because of the velocity of the reaction taking place as the epoxy is curing, it is not possible to evaluate the noise floor of the measurements during the tests.

2.4 Gelation and Shrinkage from Rheology

The gelation point, ϕ_{gel} and chemical shrinkage, ε_{sh}^{ϕ} of the curing resin are measured with a parallel plate rheometer (ARES-G2, TA Instruments) with 25 mm diameter disposable aluminum plates [3]. The resin mixture is injected between the plates ensuring an initial thickness, $h_0 = 1.5 \pm 0.05$ mm. Tests are conducted at isothermal cure temperature, $T_{cure} = 50^{\circ}\mathrm{C}$ to avoid thermal expansion effects.

For gelation measurement, the rheometer is set in a gap control mode: a constant initial gap between the plate is maintained and a zero normal for, F_N is applied. The maximum strain is set to 200% with a frequency of 1Hz in order to be in the linear viscoelastic region (LVR) of the epoxy. The response from the shearing resin is recorded as storage modulus G' and loss modulus G''. The crossover between G' and G'' is regarded as the gelation point of the resin. The complex viscosity of the resin at this point is also measured and is used to switch from gap control mode to force control mode for subsequent post-gelation shrinkage measurement. The resin is found to gel within 40 minutes of curing at $50^{\circ}\mathrm{C}$. This range is typical for infusion resins (used for RTM process), which require a long gelation time in order to maximize injection time.

The post-gelation chemical shrinkage tests are divided into two steps. The first step is gap control mode, where liquid resin is allowed to cure under zero normal force until it gels as described above. When the complex viscosity corresponds to that at gelation, the rheometer switches to force control mode. During this step, a constant force of 0.1 N, with a maximum torque of 100000 μN.m at 30 Hz frequency is applied and the variation in the gap h is measured. Assuming the in-plane strains in the resin are zero and the material is incompressible ($\nu = 0.5$), the linear variation in the gap can be converted to volumetric shrinkage using the relation below.

$$\varepsilon_{sh}^{\phi} = \left[1 + \frac{1}{3}\left(\frac{h - h_0}{h_0}\right)\right]^3 - 1 \tag{5}$$

where ε_{sh}^{ϕ} is the chemical volumetric shrinkage, h_0 is the initial gap and h is the value of the gap at a given time.

3. Results and Discussion

Three tests were conducted with 3D-DIC for each case study (post-gelation measurement and throughout curing) for a total of six experiments. Full-field strain data was collected with the ARAMIS acquisition software and further processed in MATLAB. Snapshots of the major strain evolution during curing are shown below in Figure 3 for a pre-gelation experiment and all the post-gelation tests.

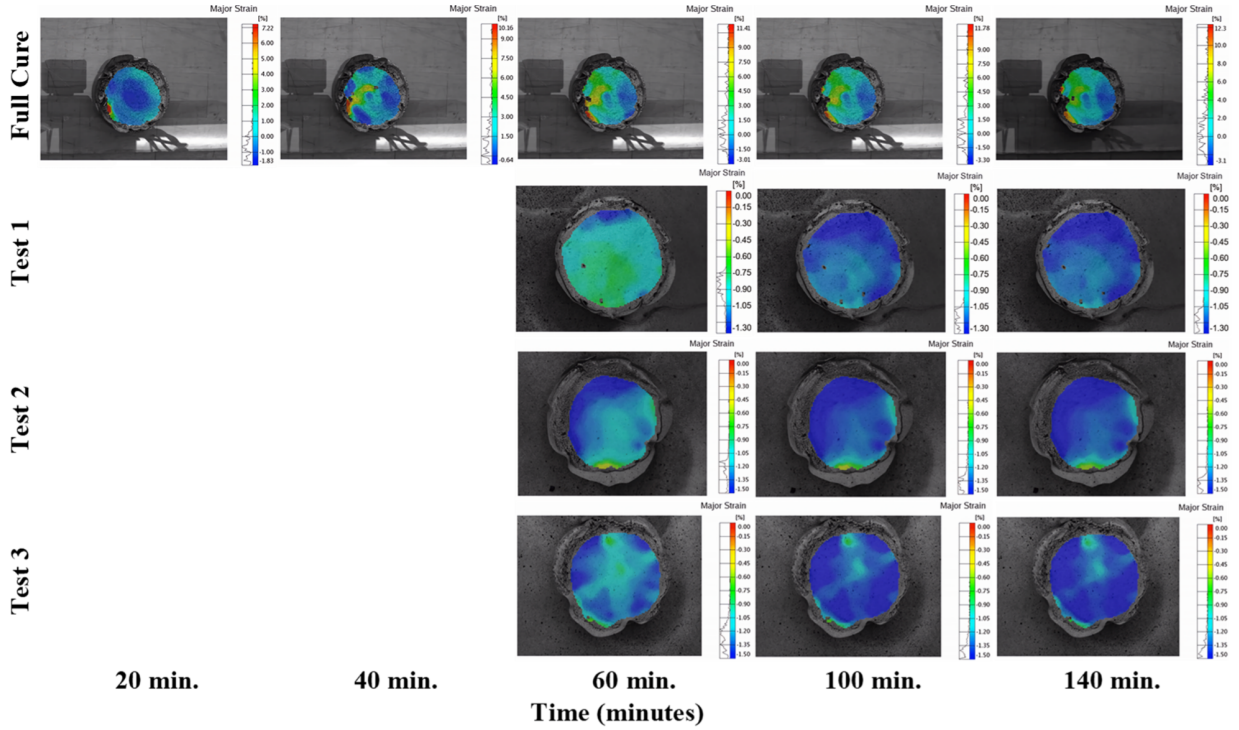

Figure 3. Visualization of the major strain obtained from 3D-DIC measurements with ARAMIS.

All post-gelation tests show a homogenous strain distribution with minor boundary effects. These boundary effects may have come from the resin mixture breaching the Teflon sheet, thus sticking to the petri dish container. Negligible areas of missing optical data were observed in the post-gelation tests. A sample size of twenty data points was used to plot the strain evolution from 3D-DIC, as shown in Figure 4.

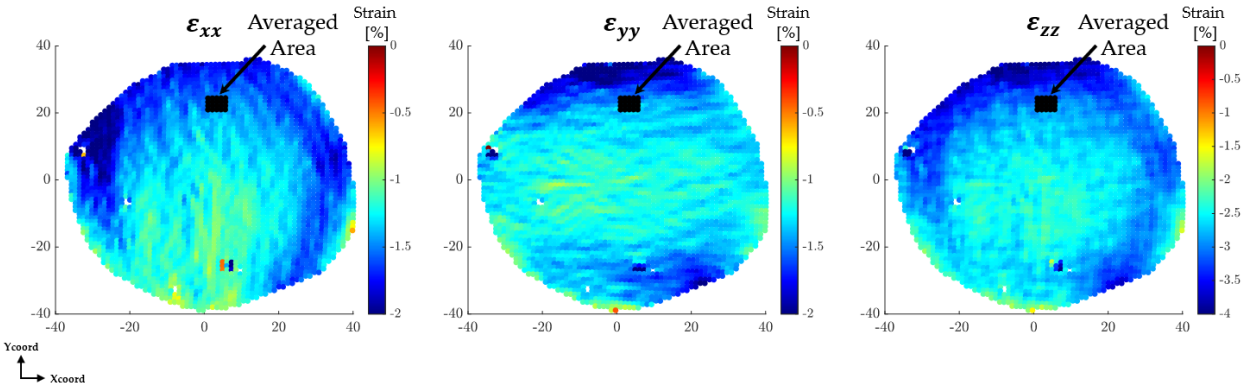

Figure 4. Post-gelation Test 1 3D-DIC strain component contours post-processed in MATLAB.

Figure 5 shows the post-gelation shrinkage plotted with the averaged volumetric shrinkage evolution from three rheology experiments. The degree of cure curve, calculated from the cure kinetics constants, is also plotted. The gelation time was determined to be approximately 41.6 minutes from rheology experiments.

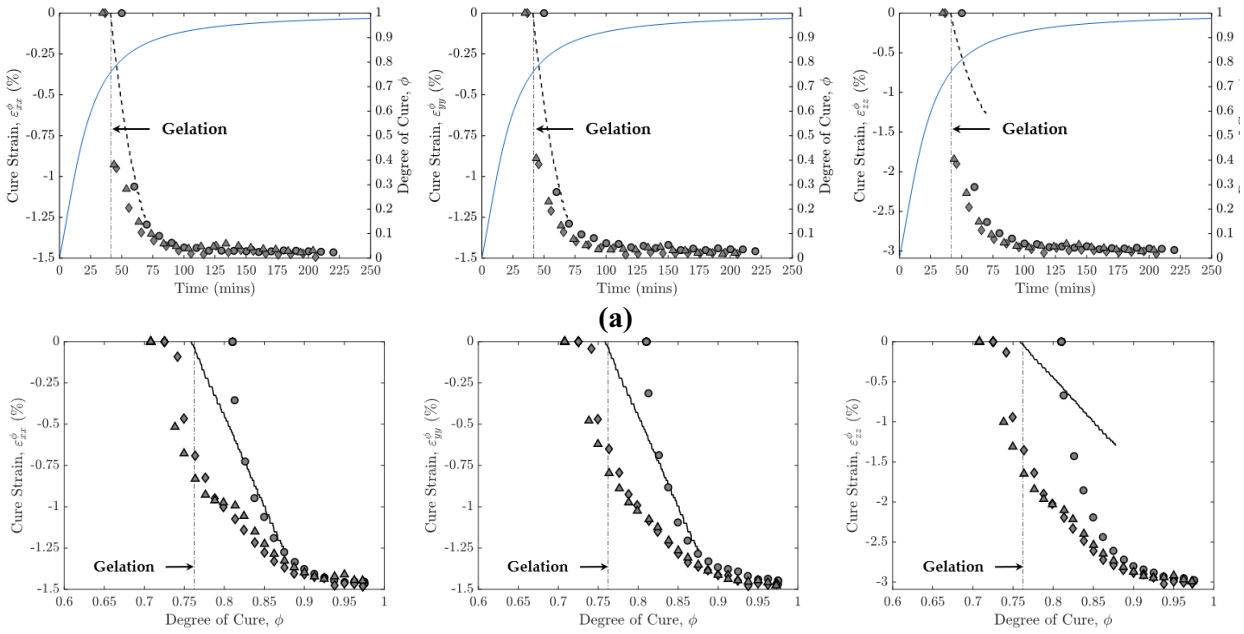

Figure 5. Post-gelation 3D-DIC strain evolution and compared with rheology for resin system EPON 862/TETA plotted against (a) time and (b) degree of cure.

Figure 5 shows that the in-plane strains from 3D-DIC compare quite well with each other and with rheology. However, the final out-of-plane 3D-DIC strains (~3%) are approximately twice as high as the in-plane (~1.5%). This is because 3D-DIC experiments have a lower accuracy in the out-of-plane direction than in-plane. All three tests show that most of the shrinkage occurred within the first 35-40 minutes of the image acquisition. Figure 5(b) shows that the cure shrinkage produced from rheology evolves perfectly linearly with respect to degree of cure. This is because the rheology experiment assumes plane-strains in the resin are zero and only extrapolates strain from the out-of-plane direction. The 3D-DIC experiments make no such assumptions, and thus show a slightly nonlinear relationship between shrinkage and degree of cure.

The strain evolution from the post-gelation tests were then compared to those from the pre-gelation case as shown in Figure 6, where the post-gelation curves have been overlapped to the three to compare shrinkage trends as a function of degree of cure between the pre-gelation and the post-gelation measurements.

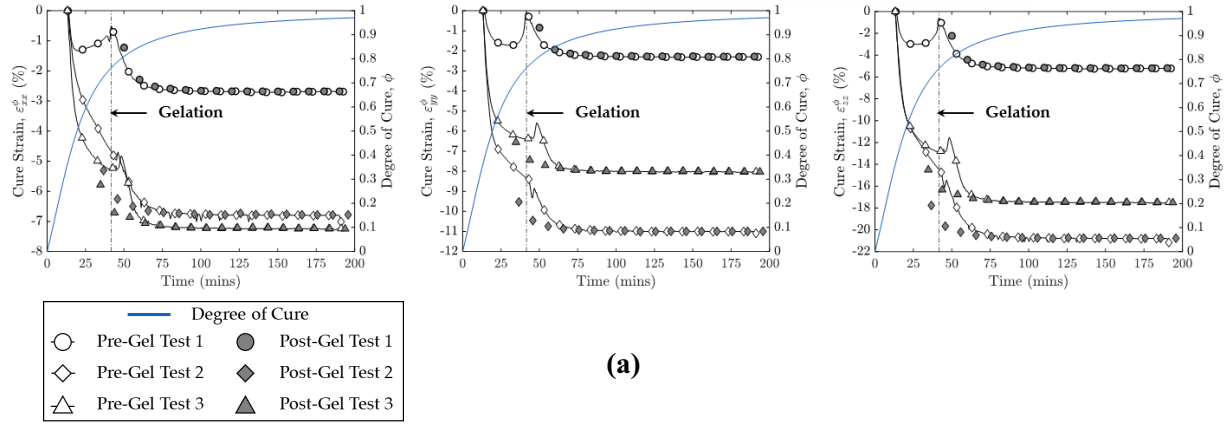

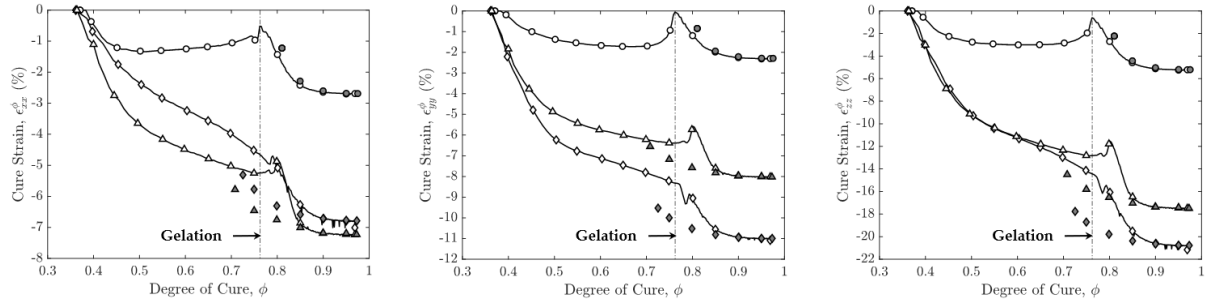

(b)

Figure 6. Pre- and post-gelation 3D-DIC experiments for resin system EPON 862/TETA plotted against (a) time and (b) degree of cure. Note that the post-gelation final shrinkage values have been shifted to match those of their respective pre-gelation tests.

It is clear from Figure 6 that the pre-gelation strain is not negligible. One test shows that the rate of strain evolution is negative at the start of the experiment but then becomes positive approximately 10 minutes prior to gelation and peaks at gelation. After gelation, the strain evolution shows a similar trend to those from the post-gelation tests. Two of the tests that exhibited paint cracking during curing also show a significant drop in strain at the start of the experiment as seen in Figure 7(b-c).

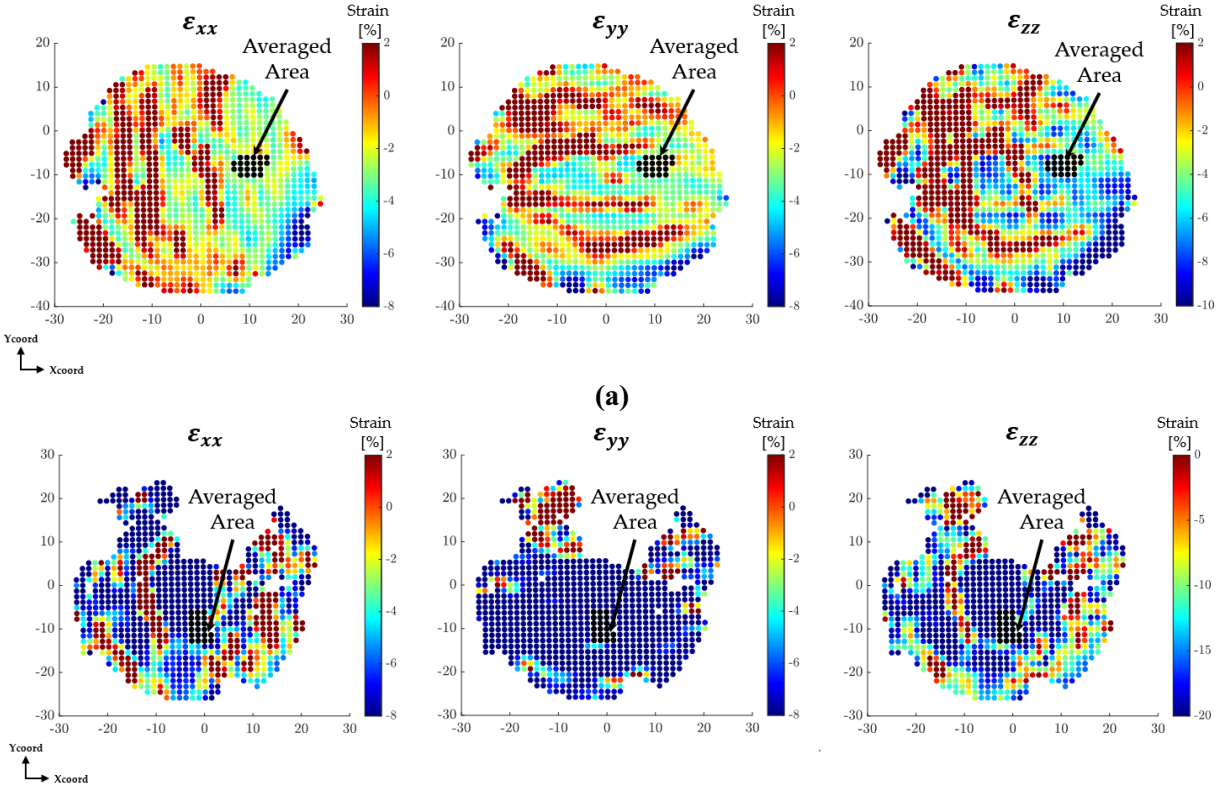

(a)

(b)

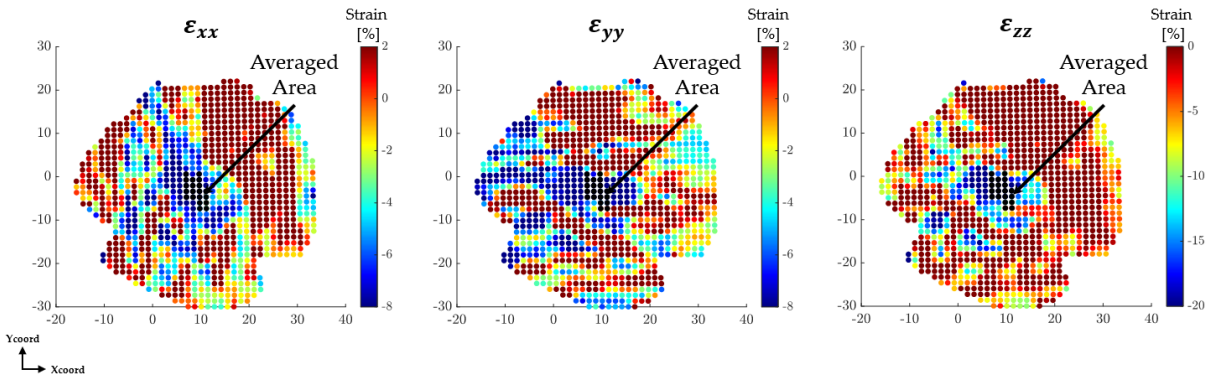

(c)

Figure 7. Pre-gelation 3D-DIC strain component contours post-processed in MATLAB for (a) Test 1; (b) Test 2; and (c) Test 3.

There are localized peaks that occur after gelation, at which point the strain evolution follows a similar trend seen in post-gelation experiments. Furthermore, due to the paint cracking and boundary effects that were experienced in these pre-gelation tests, the strain evolution may be representative of the macroscopic behavior of the resin rather than the chemical shrinkage inherent in the material. There is also more variability in between the in-plane and out-of-plane strain behavior for the pre-gelation case. This is because more of the cure reaction was captured, thus creating more opportunity for variability due to imperfections such as boundary effects and cracking. The pre-gelation tests demonstrate how the in-situ shrinkage evolution during curing is highly dependent on the mechanical constraint imposed by the curing geometry or by the presence of reinforcements, such as carbon or glass fibers.

4. Conclusions

A novel approach to measure chemical shrinkage with three-dimensional digital image correlation (3D-DIC) for resin system EPON 862/TETA was introduced in this work. This new method was demonstrated for the post-gelation and pre-gelation curing. Post-gelation strain component results show excellent in-plane agreement with rheology experiments. Pre-gelation experiments showed a non-negligible strain evolution prior to gelation and a larger variability between in-plane strains that highly depends on the mechanical constraint acting on the resin during curing which highlight the need for computational techniques to accurately estimate the curing-induced strain evolution in composites. The accuracy of out-of-plane 3D-DIC measurements was estimated to be factor of two for both cases.

References

[1] J. Beauson, B. Madsen, C. Toncelli, P. Brøndsted, and J. I. Bech, "Recycling of shredded composites from wind turbine blades in new thermoset polymer composites," *Composites Part A: Applied Science Manufacturing,* vol. 90, pp. 390-399, 2016.

[2] A. Dorigato, "Recycling of thermosetting composites for wind blade application," *Advanced Industrial Engineering Polymer Research,* vol. 4, no. 2, pp. 116-132, 2021.

[3] S. P. Shah, S. U. Patil, C. J. Hansen, G. M. Odegard, and M. Maiarù, "Process modeling and characterization of thermoset composites for residual stress prediction," *Mechanics of Advanced Materials Structures,* pp. 1-12, 2021.

[4] S. Ramakrishna, J. Mayer, E. Wintermantel, and K. W. Leong, "Biomedical applications of polymer-composite materials: a review," *Composites science technology,* vol. 61, no. 9, pp. 1189-1224, 2001.

[5] H. Madhav, N. Singh, and G. Jaiswar, "Thermoset, bioactive, metal–polymer composites for medical applications," in *Materials for biomedical engineering*: Elsevier, 2019, pp. 105-143.

[6] A. Iftekhar, "Biomedical composites," *Standard handbook of biomedical engineering design,* pp. 1-17, 2004.

[7] T. Biswal, S. K. BadJena, and D. Pradhan, "Synthesis of polymer composite materials and their biomedical applications," *Materials Today: Proceedings,* vol. 30, pp. 305-315, 2020.

[8] A. Badria, D. J. Hutchinson, N. Sanz del Olmo, and M. Malkoch, "Acrylate-free tough 3D printable thiol-ene thermosets and composites for biomedical applications," *Journal of Applied Polymer Science,* vol. 139, no. 43, p. e53046, 2022.

[9] L. Hollaway, "A review of the present and future utilisation of FRP composites in the civil infrastructure with reference to their important in-service properties," *Construction building materials,* vol. 24, no. 12, pp. 2419-2445, 2010.

[10] S. Das, *The cost of automotive polymer composites: a review and assessment of DOE's lightweight materials composites research*. Oak Ridge National Laboratory Oak Ridge, TN, USA, 2001.

[11] J. A. T. Palmer, "Mechanical recycling of automotive composites for use as reinforcement in thermoset composites," University of Exeter, 2009.

[12] K. Friedrich and A. A. Almajid, "Manufacturing aspects of advanced polymer composites for automotive applications," *Applied Composite Materials,* vol. 20, pp. 107-128, 2013.

[13] C. Soutis, "Fibre reinforced composites in aircraft construction," *Progress in aerospace sciences,* vol. 41, no. 2, pp. 143-151, 2005.

[14] K. B. Katnam, L. Da Silva, and T. Young, "Bonded repair of composite aircraft structures: A review of scientific challenges and opportunities," *Progress in Aerospace Sciences,* vol. 61, pp. 26-42, 2013.

[15] R. J. D'Mello, A. M. Waas, M. Maiaru, and R. Koon, "Integrated computational modeling for efficient material and process design for composite aerospace structures," in *AIAA Scitech 2020 Forum*, 2020, p. 0655.

[16] S. Shah, S. Patil, P. Deshpande, A. Krieg, K. Kashmari, H. Al Mahmud, J. King, G. M. Odegard, and M. Maiaru, "Multiscale modeling for virtual manufacturing of thermoset composites," in *AIAA Scitech 2020 Forum*, 2020, p. 0882.

[17] M. Maiaru, "Effect of uncertainty in matrix fracture properties on the transverse strength of fiber reinforced polymer matrix composites," in *2018 AIAA/ASCE/AHS/ASC Structures, Structural Dynamics, and Materials Conference*, 2018, p. 1901.

[18] S. SHAH and M. MAIARU, "Microscale analysis of virtually cured polymer matrix composites accounting for uncertainty in matrix properties during manufacturing," in *Proceedings of the American Society for Composites Thirty-third Technical Conference*, 2018.

[19] S. P. Shah and M. Maiarù, "Effect of manufacturing on the transverse response of polymer matrix composites," *Polymers,* vol. 13, no. 15, p. 2491, 2021.

[20] P. Deshpande, S. Shah, S. Patil, K. Kashmari, M. Olaya, G. Odegard, and M. Maiaru, "Multiscale Modelling of the cure process in thermoset polymers using ICME," in *Proceedings of the American Society for Composites Thirty-fifth Technical Conference*, 2020.

[21] S. PATIL, S. SHAH, P. DESHPANDE, K. KASHMARI, M. OLAYA, G. ODEGARD, and M. MAIARU, "Multi-scale Approach to Predict Cure-Induced Residual Stresses in an Epoxy System," in *Proceedings of the American Society for Composites Thirty-fifth Technical Conference*, 2020.

[22] S. U. Patil, S. P. Shah, M. Olaya, P. P. Deshpande, M. Maiaru, and G. M. Odegard, "Reactive molecular dynamics simulation of epoxy for the full cross-linking process," *ACS Applied Polymer Materials,* vol. 3, no. 11, pp. 5788-5797, 2021.

[23] P. S. Gaikwad, A. S. Krieg, P. P. Deshpande, S. U. Patil, J. A. King, M. Maiaru, and G. M. Odegard, "Understanding the Origin of the Low Cure Shrinkage of Polybenzoxazine Resin by Computational Simulation," *ACS Applied Polymer Materials,* vol. 3, no. 12, pp. 6407-6415, 2021.

[24] A. Bagheri and J. Jin, "Photopolymerization in 3D printing," *ACS Applied Polymer Materials,* vol. 1, no. 4, pp. 593-611, 2019.

[25] C. W. Hull, S. T. Spence, C. W. Lewis, W. Vinson, R. S. Freed, and D. R. Smalley, "Stereolithographic curl reduction," ed: Google Patents, 1993.

[26] L. Chen, Q. Wu, G. Wei, R. Liu, and Z. Li, "Highly stable thiol–ene systems: from their structure–property relationship to DLP 3D printing," *Journal of Materials Chemistry C,* vol. 6, no. 43, pp. 11561-11568, 2018.

[27] S. K. Romberg, M. A. Islam, C. J. Hershey, M. DeVinney, C. E. Duty, V. Kunc, and B. G. Compton, "Linking thermoset ink rheology to the stability of 3D-printed structures," *Additive Manufacturing,* vol. 37, p. 101621, 2021.

[28] H. G. Bhundiya, F. Royer, and Z. Cordero, "Engineering Framework for Assessing Materials and Processes for In-Space Manufacturing," *Journal of Materials Engineering Performance,* vol. 31, no. 8, pp. 6045-6059, 2022.

[29] L. Li, B. Li, and J. Zhang, "Dopamine-mediated fabrication of ultralight graphene aerogels with low volume shrinkage," *Journal of Materials Chemistry A,* vol. 4, no. 2, pp. 512-518, 2016.

[30] Y. Nawab, N. Boyard, V. Sobotka, P. Casari, and F. Jacquemin, "A device to measure the shrinkage and heat transfers during the curing cycle of thermoset composites," in *Advanced Materials Research*, 2011, vol. 326, pp. 19-28: Trans Tech Publ.

[31] C. Li, K. Potter, M. R. Wisnom, and G. Stringer, "In-situ measurement of chemical shrinkage of MY750 epoxy resin by a novel gravimetric method," *Composites Science Technology,* vol. 64, no. 1, pp. 55-64, 2004.

[32] A. W. Snow and J. P. Armistead, "A simple dilatometer for thermoset cure shrinkage and thermal expansion measurements," *Journal of applied polymer science,* vol. 52, no. 3, pp. 401-411, 1994.

[33] S. Hoa, P. Ouellette, and T. Ngo, "Determination of shrinkage and modulus development of thermosetting resins," *Journal of composite materials,* vol. 43, no. 7, pp. 783-803, 2009.

[34] C. B. Bucknall, I. K. Partridge, and M. J. Phillips, "Mechanism of shrinkage control in polyester resins containing low-profile additives," *Polymer,* vol. 32, no. 4, pp. 636-640, 1991.

[35] H. Yu, S. Mhaisalkar, and E. Wong, "Cure shrinkage measurement of nonconductive adhesives by means of a thermomechanical analyzer," *Journal of electronic materials,* vol. 34, pp. 1177-1182, 2005.

[36] Y. Nawab, S. Shahid, N. Boyard, and F. Jacquemin, "Chemical shrinkage characterization techniques for thermoset resins and associated composites," *Journal of Materials Science,* vol. 48, pp. 5387-5409, 2013.

[37] O. G. Kravchenko, S. G. Kravchenko, A. Casares, and R. B. Pipes, "Digital image correlation measurement of resin chemical and thermal shrinkage after gelation," *Journal of Materials Science,* vol. 50, pp. 5244-5252, 2015.

[38] S. Motagi and S. Namilae, "In-situ investigation of resin shrinkage in the composite manufacturing environment," *Applied Composite Materials,* vol. 28, pp. 651-657, 2021.

[39] G. Singer, G. Sinn, H. C. Lichtenegger, S. Veigel, M. Zecchini, and R. Wan-Wendner, "Evaluation of in-situ shrinkage and expansion properties of polymer composite materials for adhesive anchor systems by a novel approach based on digital image correlation," *Polymer Testing,* vol. 79, p. 106035, 2019.

[40] M. Kamal and S. Sourour, "Kinetics and thermal characterization of thermoset cure," *Polymer Engineering Science,* vol. 13, no. 1, pp. 59-64, 1973.

[41] M. A. Sutton, J. J. Orteu, and H. Schreier, *Image correlation for shape, motion and deformation measurements: basic concepts, theory and applications*. Springer Science & Business Media, 2009.

[42] M. A. Sutton, W. Wolters, W. Peters, W. Ranson, and S. McNeill, "Determination of displacements using an improved digital correlation method," *Image vision computing,* vol. 1, no. 3, pp. 133-139, 1983.

[43] P. Luo, Y. Chao, M. Sutton, and W.-H. Peters, "Accurate measurement of three-dimensional deformations in deformable and rigid bodies using computer vision," *Experimental mechanics,* vol. 33, pp. 123-132, 1993.

[44] A. Sabato, A. Sarrafi, Z. Mao, and C. Niezrecki, "Advancements in structural health monitoring using vision-based and optical techniques," in *Proc., 7th Asia-Pacific Workshop on Structural Health Monitoring*, 2018.

[45] Baumer. (2015, March). *FWX20C NeuroCheck Edition – Digital Color Progressive Scan Camera*.